Environmental influences on the maximum quantum yield of terrestrial primary production

David Sandoval[1*], Victor Flo[1,2,3], Catherine Morfopoulos[1] and Iain Colin Prentice[1,4]

[1]Georgina Mace Centre for the Living Planet, Department of Life Sciences, Imperial College London, Ascot, UK

[2]Department of Animal Biology, Plant Biology and Ecology, Autonomous University of Barcelona (UAB), E08193 Bellaterra (Cerdanyola del Vallès), Catalonia, Spain

[3]CREAF, Ecological and Forestry Applications Research Centre, E08193 Bellaterra (Cerdanyola del Vallès), Catalonia, Spain

[4]Department of Earth System Science, Tsinghua University, Beijing, China

*Corresponding author. Email: d.sandoval17@imperial.ac.uk

Summary

- Historically, terrestrial biosphere models (TBMs) have assigned the intrinsic (maximum) quantum yield of photosynthesis (φ_0) a constant value for each plant functional type. However, experimental studies have shown that φ_0 – when measured on light-adapted leaves – depends on temperature. It is unclear whether this dependence is universal or biome-specific; how it is manifested at the ecosystem level; and how it should be represented in TBMs.
- By fitting empirical light-response curves to a global set of eddy-covariance CO_2 flux measurements and correcting for photorespiration, we inferred apparent, ecosystem-level φ_0 values and their temperature responses across a wide range of environments.

- The temperature response of apparent ecosystem-level φ_0 follows a universal bell-shaped curve. The shape of this curve does not markedly differ among biomes, but the maximum value of φ_0 decreases with increasing aridity, its temperature optimum increases with increasing growth temperature, and its sensitivity to temperature increases as growth temperature declines.
- Our model for $\varphi_0(T)$ aligns with recent theory highlighting the role of cytochrome b_6f in regulating the light reactions of photosynthesis. If implemented in TBMs, this model should allow better predictions of the responses of terrestrial ecosystem function to a warming climate.

Introduction

Uncertainties in the prediction of photosynthesis can cause large discrepancies in projections of ecosystem responses to global environmental change (Harrison *et al.*, 2021). Most current terrestrial biosphere models (TBMs) (Fisher *et al.*, 2014; Harrison *et al.*, 2021) rely on the biochemical theory of photosynthesis developed by Farquhar, von Caemmerer and Berry (FvCB) (Farquhar *et al.*, 1980a). However, despite sharing the same core equations, TBMs have implemented them using varying conceptualizations of leaf-to-canopy scaling (from leaf-level photosynthesis to ecosystem-level gross primary production, GPP), and different assumptions about the values of key parameters that are not specified by the theory (Rogers *et al.*, 2017). Hence, although TBMs based on FvCB might be expected to yield similar GPP estimates, in fact they do not. Indeed, many models show systematic differences both from one another and from accepted observational ranges, especially regarding the response of GPP to temperature (Dietze, 2014; Prentice *et al.*, 2015; Harrison *et al.*, 2021).

One cause of variation among models' GPP estimates is the value or values assigned to a parameter of particular importance for the land carbon cycle (McNeall *et al.*, 2024): the intrinsic

quantum yield of photosynthetic carbon fixation (φ_0). φ_0 is the initial slope of the light-response curve of photosynthesis under non-photorespiratory conditions (high CO_2 and low O_2 partial pressure); thus, it sets the maximum efficiency of photosynthesis (Long *et al.*, 1993; Rogers *et al.*, 2017). We use the symbol φ_0 here for the intrinsic, or maximum, quantum yield of CO_2 assimilation at low light intensity to distinguish it from φ without a subscript, which denotes the quantum yield at low light intensity under ambient partial pressures of CO_2 and O_2. Both quantities are distinct from the maximum carboxylation rate (V_{cmax}) and the maximum rate of electron transport (J_{max}) as defined in the FvCB model, whose temperature dependencies have been studied far more extensively. Research on the light reactions of photosynthesis since the 1950s has established the theoretical maximum value for φ_0 to be either 1/8 = 0.125, i.e. one mole of assimilated CO_2 requires at least eight moles of absorbed photons based on the NADPH requirement of carbon fixation (Warburg *et al.*, 1950; Emerson, 1958; Walker, 1992; Hill & Govindjee, 2014), or 1/9 ≈ 0.111 based on the ATP requirement (Evans, 1987; Long *et al.*, 1993). Almost all reported values have been obtained from measurements on leaves conducted in a non-photorespiratory atmosphere, within a narrow temperature range (25–30ºC) and with adequate water supply. Under these conditions measured φ_0 falls within the range of 0.07–0.125 mol CO_2 mol^{-1} photon, with highest values in shade-adapted plants, and lower values in C_4 compared to C_3 plants (Ehleringer & Björkman, 1977; Ehleringer & Pearcy, 1983; Björkman & Demmig, 1987; Long *et al.*, 1993; Singsaas *et al.*, 2001; Skillman, 2008).

Despite limited knowledge of how φ_0 responds to low or high temperatures and varying water availability, and how it upscales from leaves to ecosystems, it has generally been assumed that the available leaf-level observations are representative and sufficient to infer globally applicable values for modelling purposes (Walker, 1992; Long *et al.*, 1993; Singsaas *et al.*, 2001). This assumption has led to φ_0 being prescribed in TBMs as a constant value per plant functional type, with no variation with temperature (Rogers *et al.*, 2017). Empirical light use

efficiency (LUE) models that incorporate a downward regulation factor for ambient CO_2 (e.g. (Zhang *et al.*, 2019); (Bao *et al.*, 2022); (Cao *et al.*, 2022) have similarly relied on prescribed, constant maximum LUE values for each plant functional type.

The temperature (in)dependence of φ_0 can be analysed using a corollary to the FvCB model (Farquhar *et al.*, 1980b; von Caemmerer, 2000), which approximates the quantum yield of leaf-level photosynthesis at low light as follows:

$$\varphi \approx \lim_{I \to 0} \frac{\partial A}{\partial I} = \frac{c_i - \Gamma^*}{8c_i + 16\Gamma^*}(1-f)\alpha = \frac{1}{8} m_j (1-f)\alpha \qquad (1)$$

where A is the assimilation rate, I is the incident irradiance, c_i is the intercellular CO_2 partial pressure, α is the leaf absorptance, f is a correction factor for light quality (≈ 0.15: von Caemmerer, 2000) and $m_j = (c_i - \Gamma^*)/(c_i + 2\Gamma^*)$ where Γ^* is the photorespiratory compensation point, given by:

$$\Gamma^* = \frac{pO_2 K_c V_{omax}}{2K_o V_{cmax}} \qquad (2)$$

where pO_2 is the partial pressure of oxygen, $V_{_max}$ and K are the maximum rates and Michaelis-Menten coefficients respectively, and the subscripts $_o$ and $_c$ refer to oxygenation or carboxylation. Under non-photorespiratory conditions Γ^* becomes negligible; so m_j approaches 1.0, and φ_0 approaches $\frac{1}{8}(1-f)\alpha$ (Fig. 1a), independent of temperature. Under photorespiratory conditions φ is predicted only to decline with increasing temperature, due to the greater temperature sensitivity of K_o relative to K_c.

However, these predictions are inconsistent with observations. Eq. (1) generally overestimates φ at low temperatures, under both non-photorespiratory and ambient CO_2 conditions (Fig. 1b); and as noted by (Rogers *et al.*, 2019) for Arctic plants, the observed change of φ with temperature below 25˚C is opposite to that predicted, increasing rather than decreasing with temperature. This qualitative disagreement between theory and observations might explain some of the inconsistencies in the temperature responses of GPP predicted by FvCB-based TBMs (Bloomfield *et al.*, 2023).

In principle, φ_0 reflects the emergent efficiency of the whole electron-transport chain. According to a recent mechanistic description of the electron transport system (Johnson & Berry, 2021), this involves the efficiencies of both Photosystems I and II, with the cytochrome b_6f complex regulating the electron flow between the two in such a way as to minimise losses of absorbed light under low light while down-regulating electron transport (to match the use of ATP and NADPH for carboxylation) under saturating light. The different elements of the coupled photosynthetic system work in tandem and have distinct temperature dependencies (Johnson & Berry, 2021; Johnson *et al.*, 2021). In the FvCB theory, by contrast, the only temperature effect applied to the electron-transport chain is to J_{max}, which is empirically defined as the asymptotic rate of electron transport under saturating light and CO_2 (Farquhar *et al.*, 1980a; Johnson *et al.*, 2021) – implying that φ_0 is not or barely temperature-dependent, as suggested by Eq. (1).

Many empirical studies have focused on the initial stage of the electron-transport chain, the large protein complex Photosystem II, whose quantum efficiency (Φ_{PSII}), defined as the number of electrons transported per photon absorbed by PSII (as measured by pulse amplitude modulation fluorometry) is expected to be proportional to φ_0 when photosynthetic steady state

is experimentally forced by actinic light under non-photorespiratory conditions (Björkman & Demmig, 1987; Genty *et al.*, 1989; Oberhuber *et al.*, 1993). When measured on dark-adapted leaves, Φ_{PSII} shows little or no temperature dependence. In light-adapted leaves, however, Φ_{PSII} typically shows a distinct bell-shaped response to temperature (Fig. 1c) in both C_3 and C_4 species (Dwyer *et al.*, 2007). Fig. 1 also shows data (or empirical models fitted to data) on φ_0 (panel a), derived from CO_2 assimilation measured under non-photorespiratory conditions, and φ (panel b), from CO_2 assimilation under ambient conditions – indicating a range of responses to temperature but broadly suggestive of a unimodal pattern similar to that shown for Φ_{PSII} in panel c.

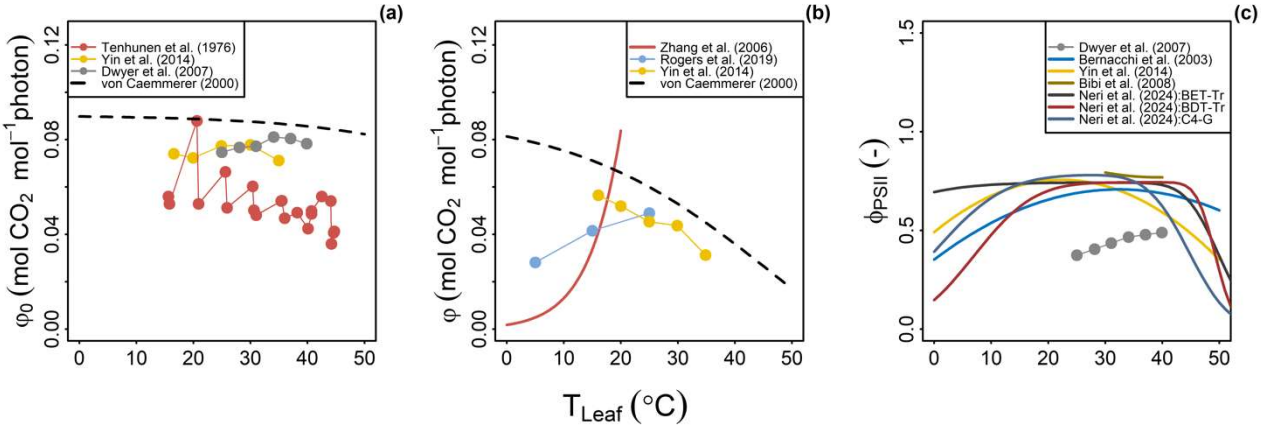

Fig. 1. Maximum quantum yield responses to temperature from various sources. Connected dots represent observations, solid lines represent empirical models fitted to observations, and dashed lines represent predictions from the FvCB theory (Eq. (1)). **(a)** Non-photorespiratory maximum quantum yield of CO_2 assimilation (Tenhunen *et al.*, 1976b; von Caemmerer, 2000; Dwyer *et al.*, 2007; Yin *et al.*, 2014); Eq. (1) forced here with CO_2 set at 750 µmol mol^{-1} and 2% O_2. **(b)** Ambient maximum quantum yield of CO_2 assimilation (von Caemmerer, 2000; Zhang *et al.*, 2006; Yin *et al.*, 2014; Rogers *et al.*, 2019); Eq. (1) forced here with CO_2 set at 400 µmol mol^{-1} and 21% O_2. **(c)** Quantum yield of Photosystem II in light-adapted leaves from different studies (Bernacchi *et al.*, 2003; Dwyer *et al.*, 2007; Bibi *et al.*, 2008; Yin *et al.*, 2014; Neri *et al.*, 2024). Selected PFTs from Neri *et al.* (2024): BET-Tr, broadleaf evergreen tropical tree; BDT-Tr, broadleaf deciduous tropical tree; C4-G, C4 grass.

The large differences among the various published apparent quantum yield responses of φ_0 and φ to temperature, the limited temperature range of many data sets at leaf-scale, and the disagreement between standard theory predictions and observations suggest that a more comprehensive global analysis would be helpful for the representation of φ_0 in TBMs. Here we derive

apparent, ecosystem-level values of φ, and thence φ_0, from the slopes at low light of the light-response curves of net ecosystem exchange (NEE) as observed across the global network of eddy-covariance flux towers. We fit a universal empirical model to this response, and show how the model's parameters are influenced by adaptation to different growth environments.

Materials and methods

We exploited the abundance of half-hourly NEE data available from eddy-covariance CO_2 flux measurements, together with *in situ* observations of the fraction of absorbed photosynthetic active radiation (fAPAR) made at 53 sites in the Ameriflux network (Novick *et al.*, 2018). We estimated fAPAR from measured above- and below-canopy Photosynthetic Photon Flux Density (PPFD, μmol m^{-2} s^{-1}) as follows (Carrara *et al.*, 2018):

$$fAPAR = \frac{PPFD_{\mathrm{IN}} - PPFD_{OUT} - PPFD_{BC_{\mathrm{IN}}}(1 - \alpha_{soil})}{PPFD_{\mathrm{IN}}} \quad (3)$$

where $PPFD_{IN}$ is the incoming (incident) PPFD and $PPFD_{OUT}$ the outgoing PPFD at the top of the canopy, and $PPFD_{BCIN}$ is the incoming PPFD below the canopy. α_{soil} is the soil albedo in the visible light spectrum, taken here as 0.17 (Feister & Grewe, 1995). Absorbed PPFD (I_{abs}) was estimated as the product of $PPFD_{IN}$ and fAPAR. We additionally used a larger, globally distributed set of 310 sites (Pastorello *et al.*, 2020; Hufkens, 2022; Ukkola *et al.*, 2022) using remotely sensed fAPAR (Myneni *et al.*, 2015) from the MODIS MCD15A3 product (Myneni *et al.*, 2015), interpolated to daily timesteps.

For each site, we estimated φ_0 values within 1°C temperature bins using Nonlinear Least Squares. To capture the maximum efficiency and avoid limitations caused by factors other than temperature and light (e.g. soil moisture), we used only the upper envelope (95th percentile) of

the data; and only data points flagged as daytime good-quality observations were used. To account for the curvature of the light-response curve and ecosystem respiration (Re), we fitted the following hyperbolic equation to the NEE data (Smith, 1937; Stocker *et al.*, 2020):

$$-NEE = A - \mathrm{Re} = \varphi_0 \frac{I_{\mathrm{abs}} m_{\mathrm{j}}}{\sqrt{1+\left(\frac{\varphi_0 I_{\mathrm{abs}}}{A_{\mathrm{sat}}}\right)^2}} - \mathrm{Re} \tag{4}$$

where A_{sat} is the asymptotic value of GPP under saturating light. The factor m_{j} corrects for photorespiratory conditions and the effect of vapour pressure deficit (D) on stomatal opening, following the least-cost hypothesis:

$$m_{\mathrm{i}} = \frac{c_i - \Gamma^*}{c_i + 2\Gamma^*} = \frac{c_a - \Gamma^*}{c_a + 2\Gamma^* + 3\Gamma^* \sqrt{\frac{1.6\eta^* D}{\beta(K+\Gamma^*)}}} \tag{5}$$

where c_{a} is the ambient partial pressure of CO_2; $K = K_{\mathrm{c}}(1 + pO_2/K_{\mathrm{o}})$ is the effective Michaelis constant of Rubisco; η* is the viscosity of water, normalised by its value at 25˚C; D is the vapour pressure deficit; and β is a constant, estimated as 146 (Stocker et al., 2020) based on global leaf $\delta^{13}C$ data. The method is illustrated in Fig. 2.

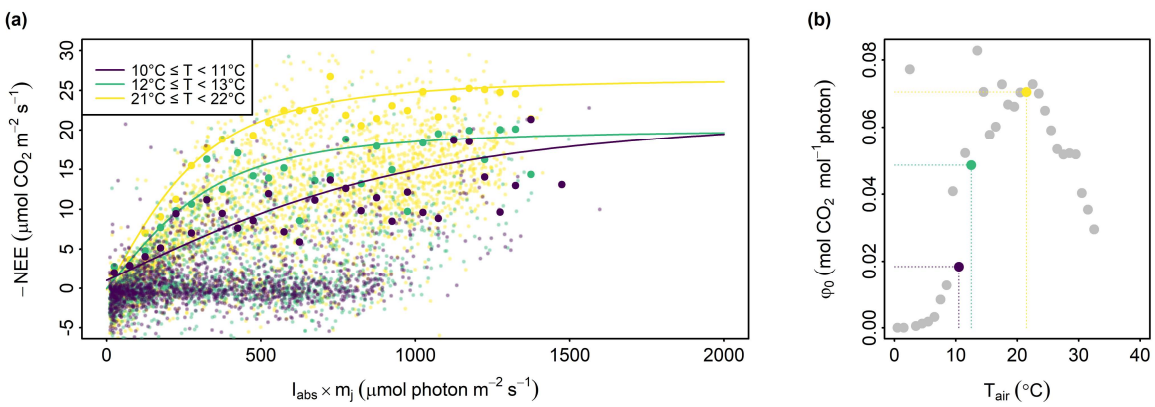

Fig. 2. Method used to extract $\varphi_0(T)$. Three 1.0 °C intervals with different colours are shown as an example for the Harvard Forest site US-xHa (Biome: deciduous broadleaf forest, mean annual temperature = 6.6 °C, mean annual precipitation = 1071 mm). **(a)** Point clouds per

temperature bin: larger points denote the 95th percentile, and solid lines are Eq. (4) fitted to these 95th percentiles. **(b)** φ_0 extracted from the fitted Eq. (4) as shown in panel **(a)**.

Once φ_0 was found at each temperature bin, we fitted $\varphi_0 = f(T)$ to a peaked Arrhenius equation (Eq. 6-7; Kattge & Knorr, 2007) by using the classic Nelder–Mead optimization algorithm (Nelder & Mead, 1965) with the Nash–Sutcliffe (NSE) coefficient (Nash & Sutcliffe, 1970), which relates the variance of the residuals to the variance of the data as the objective function, then we repeated this procedure for all sites:

$$T_{opt} = \frac{H_d}{\Delta S - R log\left(\frac{H_a}{H_d - H_a}\right)} \quad (6)$$

$$\varphi_0(T) = \widehat{\varphi_0} \frac{H_d \, exp\left(\frac{H_a\left(T_{air} - T_{opt}\right)}{T_{air} \, R \, T_{opt}}\right)}{H_d - H_a\left(1 - exp\left(\frac{H_d\left(T_{air} - T_{opt}\right)}{T_{air} \, R \, T_{opt}}\right)\right)} \quad (7)$$

where T_{opt} (K) is the temperature at the peak, H_a (J mol^{-1}) is the activation energy, H_d (J mol^{-1}) the deactivation energy, ΔS (J mol^{-1} K^{-1}) is the entropy change between the ground and transition states of the reaction, $\widehat{\varphi_0}$ is the intrinsic quantum yield at T_{opt}, and R (J mol^{-1} K^{-1}) is the universal gas constant.

To test whether the site's bioclimate shapes this response to temperature, we fitted nonlinear models using bioclimatic indices explaining ΔS, T_{opt} and $\widehat{\varphi_0}$ parameters from the peaked Arrhenius equation with 10 000 bootstrap resampling iterations. The bioclimatic metrics tested were aridity index ($AI = PET/P$), evaporative index ($EI = ET/P$), evaporative fraction ($EF = ET/PET$) and mean temperature during growth days (mGDD$_0$) where PET is the mean annual potential evapotranspiration, P is mean annual precipitation, and ET is the mean annual

actual evapotranspiration. PET was estimated using the SPLASH v2.0 model (Sandoval *et al.*, 2024), which accounts for surface temperature feedback on the net radiation. Actual evapotranspiration was estimated by converting the latent heat observed at the tower using the latent heat of vaporisation with corrections for local temperature and pressure. Growth days are defined as days with mean temperatures > 0ºC. Mean growth temperature ($mGDD_0$) was estimated as the average temperature during those days. All the environmental data used to estimate the bioclimatic metrics were measured *in situ*, except for sites where the records were shorter than five years. In such cases, data from ERA5 (Muñoz-Sabater, 2019) were used instead.

To compare our model, theoretical simulations of φ_0 were carried out using the model and code described in (Johnson *et al.*, 2021) with default parameters for *Populus fremontii* as used in (Johnson & Berry, 2021). Bioclimatic metrics for the sites described in (Johnson & Berry, 2021) and (Rogers *et al.*, 2019) were calculated using data from ERA5 (Muñoz-Sabater, 2019) and SPLASH v2.0 (Sandoval *et al.*, 2024). To evaluate the effect of the new formulation on global GPP $\varphi_0(T)$ was implemented in the P model and global simulations were run with both the original which applies Bernacchi *et al.* (2003) $\varphi_0(T)$ correction, and the new formulation.

Results

φ_0 varied considerably across biomes and climate zones. Mean values showed a smooth transition between biomes, with higher values in forests and lower values in grasslands and shrublands (Fig. 3a). Examining this transition using climate zones, a marked pattern emerged, driven by the aridity gradient. Tropical rainforest (Af) and tropical monsoon (Am) climates appeared at the upper end of the φ_0 axis, followed by sites with “no dry season” (*f* types), and then by sites with dry/wet seasonality (*w* and *s* types). Finally, sites from arid climates

(BW*) and steppe appeared in the lower end (BS*) (Fig. 3b and 3c).

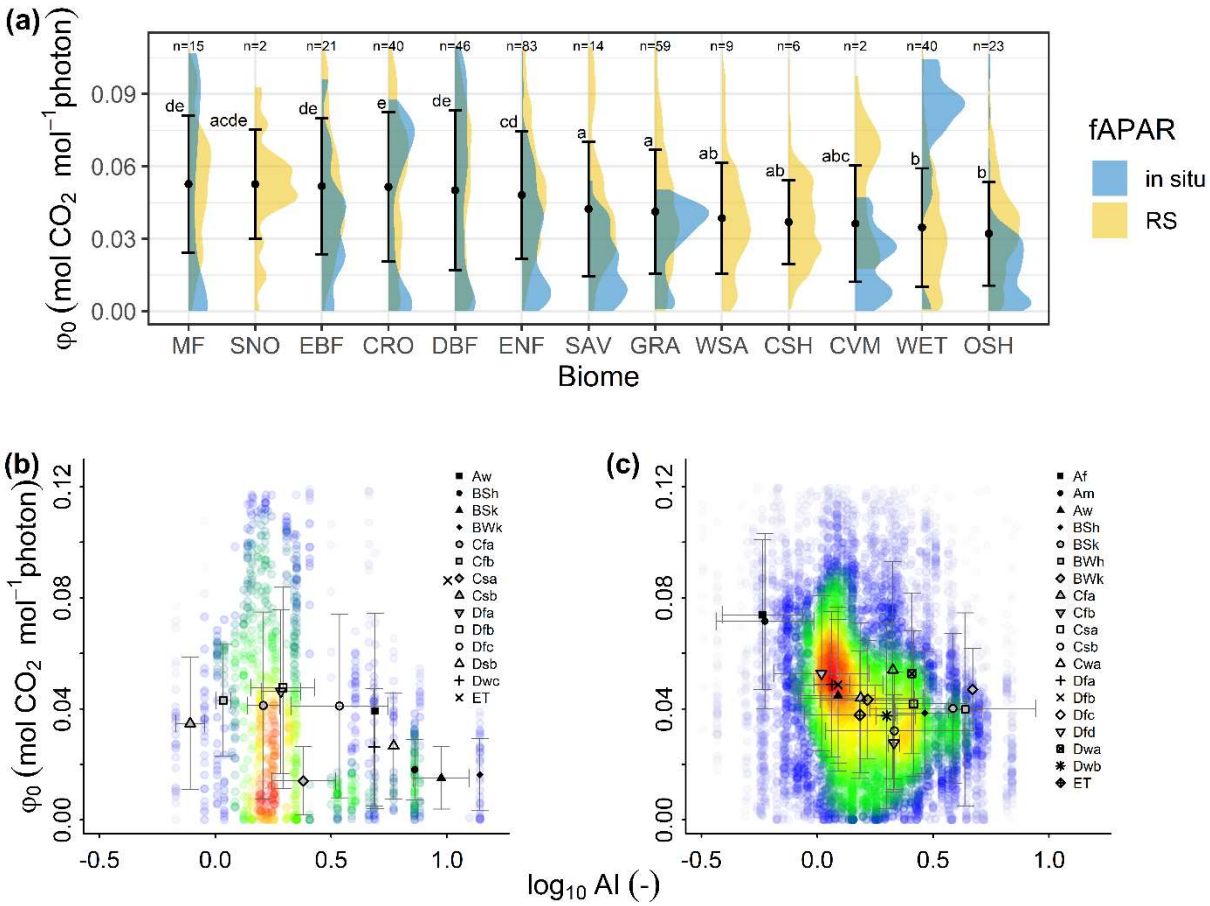

Fig. 3. Observed φ_0 inferred by using *in situ* and remotely sensed fAPAR. (a) Probability distribution of φ_0 per biome and fAPAR source. The symbols and the black bars denote the mean and standard deviation per biome, based on combined fAPAR sources. Post hoc Tukey test results at the top of the bars and the number of sites at the top of the distributions. **(b)** φ_0 as a function of aridity index from in situ fAPAR sites. **(c)** φ_0 as a function of aridity index from RS fAPAR sites. Symbols in panels **b** and **c** show the average φ_0 values per climate zone and the colours denote point density.

The response of φ_0 to temperature showed a bell-shaped pattern across all sites (Fig. 4a). In general, the average φ_0 steadily increased up to a maximum, followed by a sharper drop. This pattern also emerged using the 75th and 95th percentiles of φ_0 (Fig. 4a). The global maximum efficiency, defined based on the 95th percentile, was 0.111 ± 0.003 mol CO_2 mol^{-1} photon and was located at the optimal temperature of 20.46 ± 0.37 ºC. The bell-shaped response remained consistent across biomes with the in situ fAPAR data, while with the RS fAPAR wetlands and savannas showed inconsistencies (Fig 4b). Open shrublands (OSH) showed lower φ_0 values and lower sensitivity to T_{air}, whereas mixed forests (MF) showed the highest φ_0 values and higher sensitivity to T_{air}.

These patterns are less pronounced when the (temporally sparse) remote-sensing fAPAR data are used. In ENF, GRA and EBF biomes, remotely sensed fAPAR produces higher φ_0 at low temperatures – possibly indicating multiple optimal temperatures within each biome. In biomes where about the same temperature range was covered by both datasets (DBF, MF and OSH), the temperature sensitivity of $\varphi_0(T)$ was also similar between the datasets.

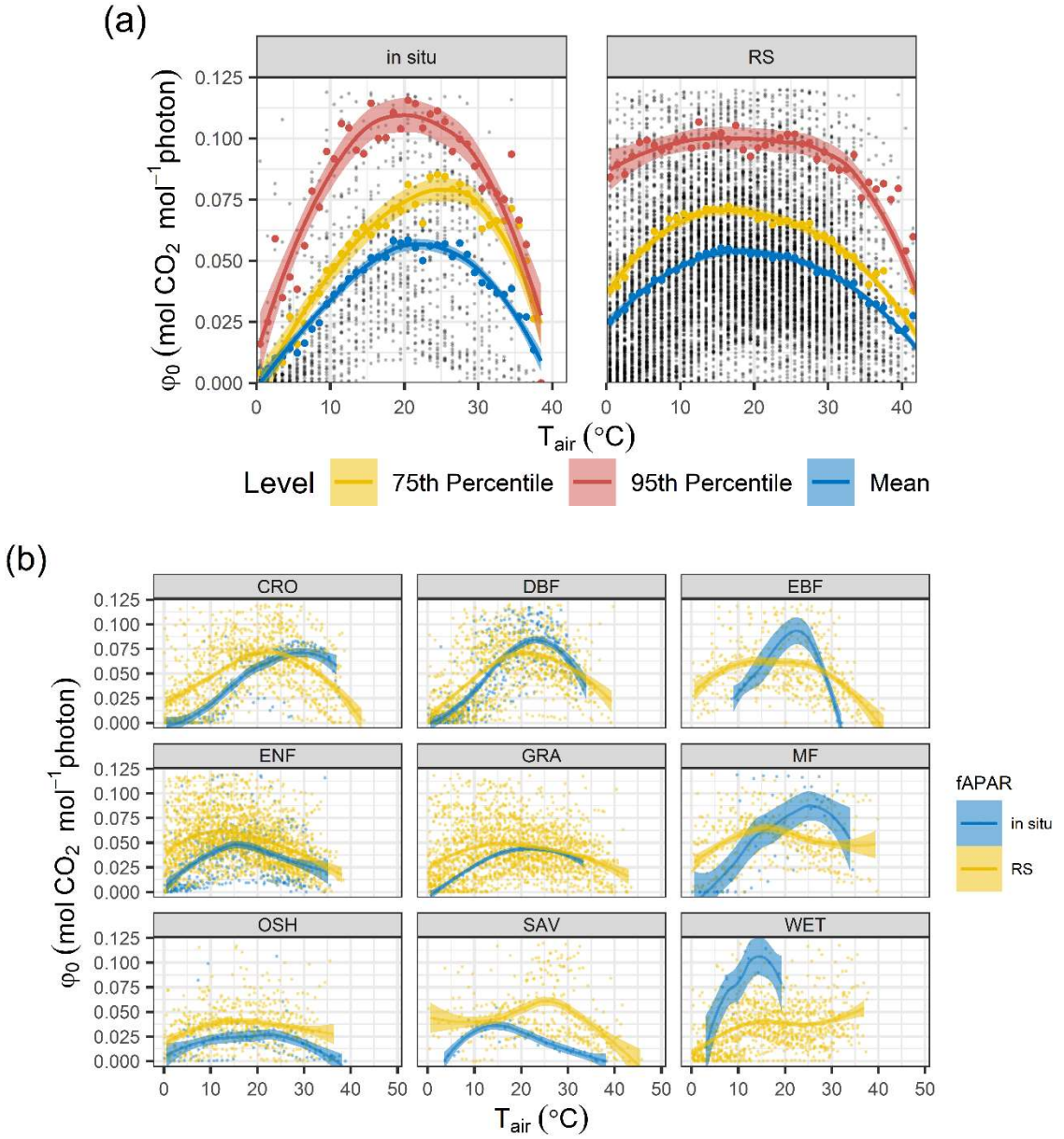

Fig. 4. φ_0 responses to temperature using all data pooled. The ribbons show a LOESS smoothing function including its 95% confidence intervals. **(a)** Pooled observations from sites with *in situ* fAPAR and sites with remotely sensed fAPAR. **(b)** Pooled observations per biome and fAPAR source.

We further analysed the temperature response at individual sites using the fitted peaked Arrhenius curves. The shapes of the response were consistent regardless of the location, biome or fAPAR source. However, different temperature sensitivities and optimal temperatures emerged. For example, wetlands (WET) as depicted in Figure 5 show the extreme difference between a wetland in the Peruvian rain forest (PE-QFR) and a wetland in Greenland (GL-Zaf).

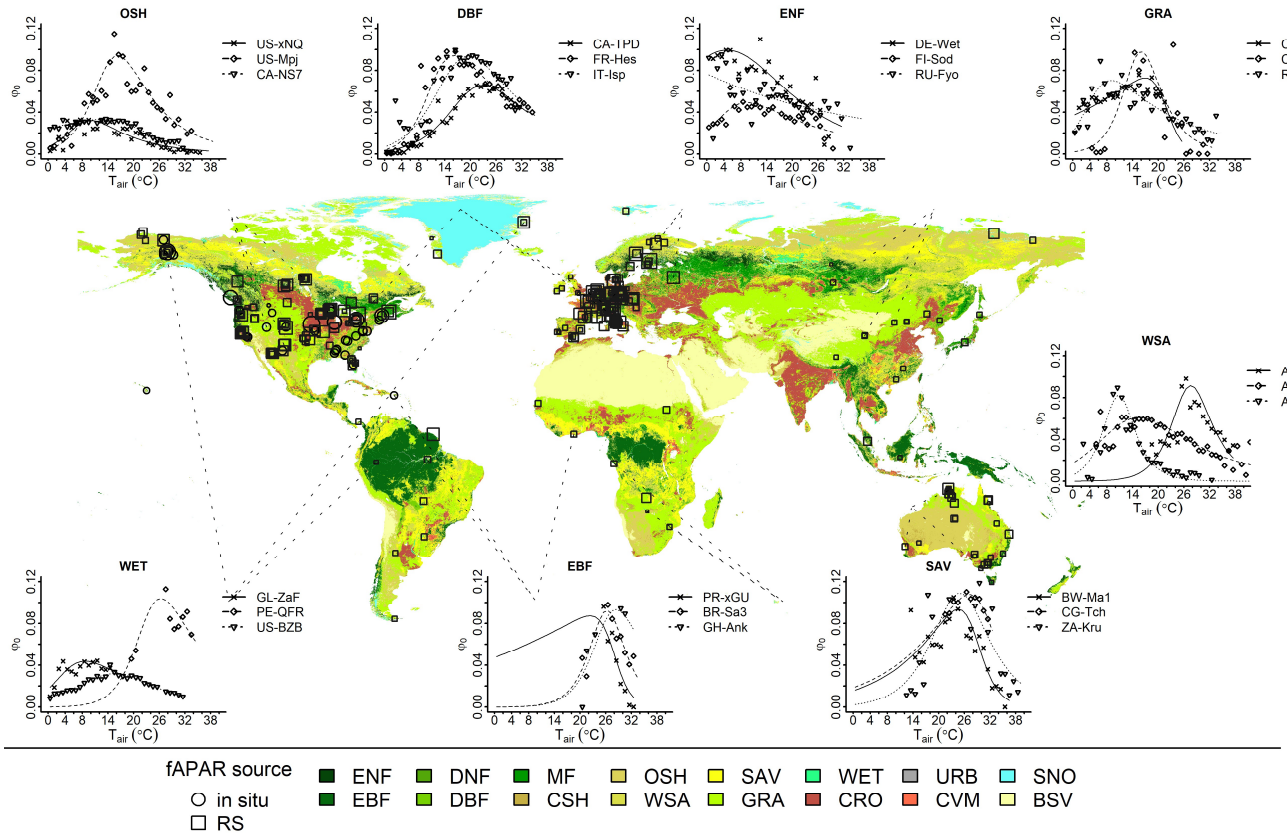

Fig. 5. φ_0 responses to temperature using peaked-Arrhenius curves. Observation (points) and predictions (lines) from selected sites.

Globally, the curves fitted site by site to the peaked Arrhenius equation were able to explain $\varphi_0(T)$ with reasonably good accuracy. Performance was slightly better for the *in situ* fAPAR, explaining 85% of the variation while explaining 72% of the variation for the *RS* fAPAR. Most of the mean values (observed and simulated) for biomes fell close to the 1:1 line, except for OSH which was slightly overestimated and WET underestimated (Fig. 6a).

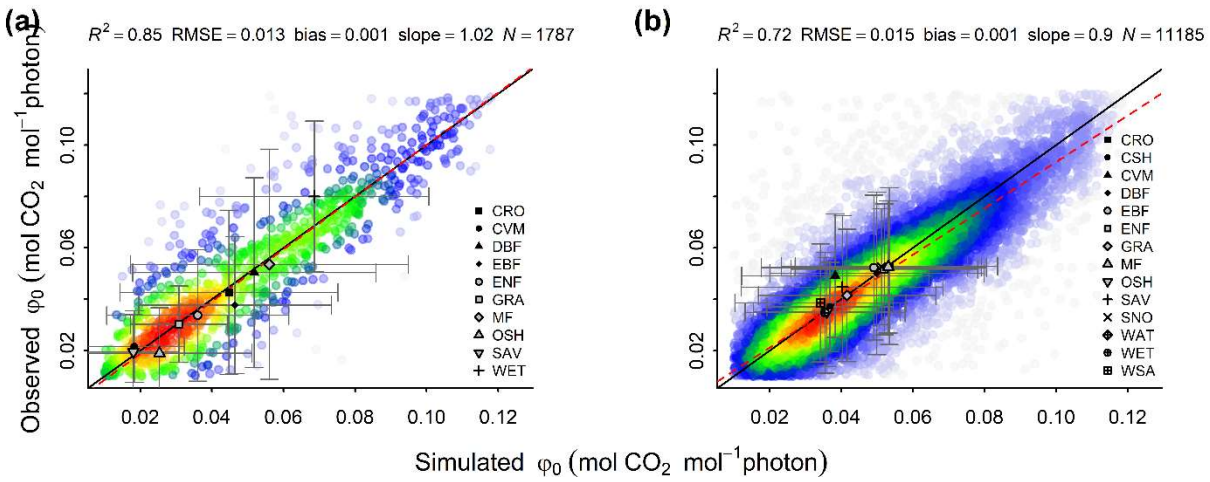

Fig. 6. Correlations of observed and simulated $\varphi_0(T)$ using peaked Arrhenius curves. (a) using *in situ* fAPAR observations. **(b)** using remotely sensed fAPAR observations. Colours denote point density.

The peak φ_0 ($\widehat{\varphi_0}$) showed considerable variation among sites, while H_a was relatively stable among sites. For most (350 sites) H_a was ~ 70.9 kJ mol^{-1}. H_d varied from ~ 111 kJ mol^{-1} to 351 kJ mol^{-1}, while ΔS varied from ~ 0.2 kJ mol^{-1} K^{-1} to >1.5 kJ mol^{-1} K^{-1} and was highly correlated to H_d. $\widehat{\varphi_0}$ decreased from a plateau when AI ≤ 1 with increasing aridity following an inverse sigmoid response (Eq. 8):

$$\widehat{\varphi_0} = \frac{0.111}{(1 + AI^m)^n} \qquad (8)$$

where m = 4.09 (95% CI: 4.07 - 9.99) and n = 0.12 (95% CI: 0.050 - 0.169). Thus $\widehat{\varphi_0}$ shows a steep decay from 0.111 when AI > 1, stabilizing (when AI > 8) at a value around 0.03 (Fig. 7a). Some of the sites that fall outside the 95% confidence intervals are tagged in the plots and discussed in the next section. The global average of $\widehat{\varphi_0}$, according to the prediction from equation (12) (Fig. 7b), was 0.08 mol CO_2 mol^{-1} photon.

ΔS decreases non-linearly, approaching stability for $mGDD_0$ > 30 ºC, as described by Eq. (9), where ΔS_0 = 3468.2 (95% CI: 1523.9 – 6408.2) and kS = -0.668 (95% CI: 0.321 - 0.639):

$$\Delta S = \Delta S_0 mGDD_0^{kS} \qquad (9)$$

Thus, replacing Eq. (9) in Eq. (6) produces T_{opt} within a range from ~17 ºC in boreal regions to ~26 ºC in the tropics (Fig. 7d), which also results in a rate of change $\frac{\Delta T_{opt}}{\Delta mGDD_0} = 0.35$.

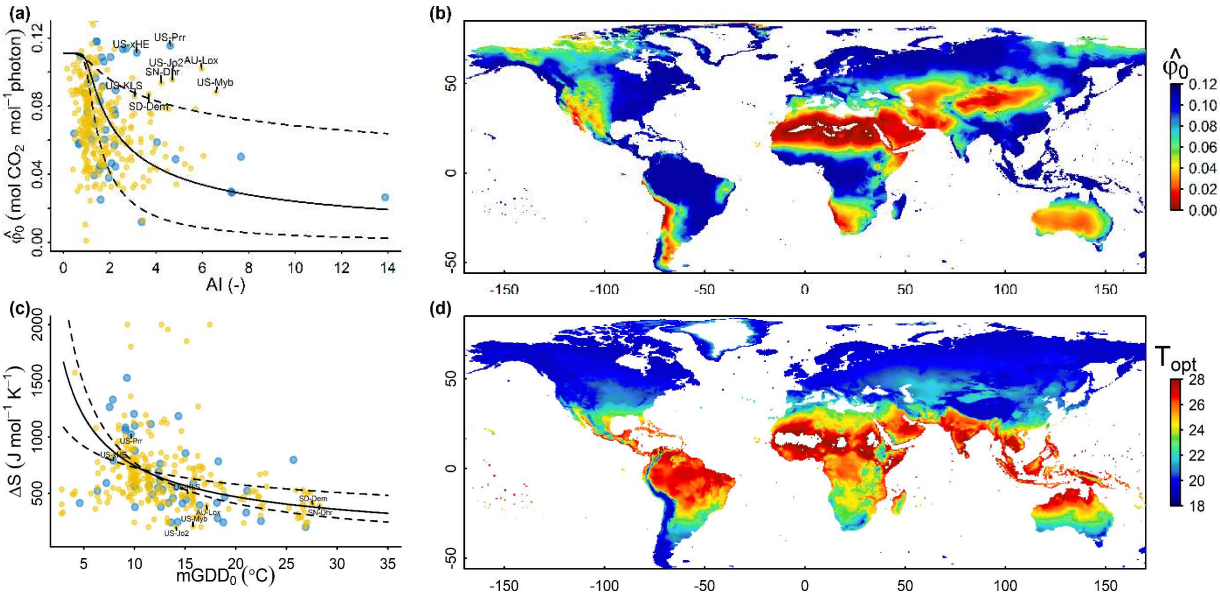

316

317 **Fig. 7. Bioclimatic patterns of the peaked Arrhenius parameters**. The colours in the scatter

318 plots refers to fAPAR measured *in situ* or from remote sensing. **(a)** $\hat{\varphi}_0$ response to aridity: solid

319 line regression, dashed lines 95% confidence intervals. **(b)** Global prediction of $\hat{\varphi}_0$ using equa-

320 tion (8). **(c)** Entropy change (ΔS) variation with growth temperature: solid line regression,

321 dashed lines 95% confidence intervals. **(d)** Global prediction of optimum temperature for φ_0

322 using equation (9).

323

Discussion

We derived apparent φ_0 at the ecosystem level for globally distributed sites, using half-hourly *in situ* measurements of fAPAR and eddy-covariance measurements of CO_2 exchange. We found that it shows a bell-shaped response with temperature, and this pattern remains consistent across all individual sites analysed, even when remotely sensed fAPAR was used in the absence of *in situ* fAPAR measurements (Fig. 5). However, this pattern was less consistent when the data were grouped per biome (Fig. 4b), suggesting that the temperature response curve for φ_0 is not biome-specific but instead gradually modulated by bioclimate. In particular, increasing aridity reduces $\widehat{\varphi_0}$, while higher growth temperatures shift the optimum temperature upward and simultaneously decrease the sensitivity of φ_0 to instantaneous temperature. The use of absorbed rather than incident radiation should implicitly account for the effect of high diffuse fractions during low sun angles and their confounding effect with low temperatures. This effect should be clearer with the *in situ* fAPAR observations, which are higher under greater diffuse light, independently of temperature. Since MODIS overpasses occur at 10:30 and 13:30, it is unlikely that they captured early-morning periods of high diffuse light and their effect on fAPAR. However, this remains a caveat, as no data were available on the partitioning between diffuse and direct radiation.

No previous studies have reported φ_0 at ecosystem scale. However in our analysis, the fitted maximum value of φ_0 (0.111 mol CO_2 mol^{-1} photon) is identical to the theoretical maximum limited by ATP generation of 0.111 (Long *et al.*, 1993) and to the maximum observed by (Walker, 1992). It also closely matches other values reported for single leaves under unstressed conditions including (Björkman & Demmig, 1987) (0.106 on average for C3 plants and 0.112 for conifers), (Skillman, 2008) (0.106) and (Singsaas *et al.*, 2001) (0.108).

Our analyses show that φ_0 is generally higher in forests, followed by grasslands and shrublands, suggesting that φ_0 varies among species from different life forms – in line with the observations by (Singsaas *et al.*, 2001), who noted that even a 100% variation in photorespiration plus alternative electron sinks could not fully explain the observed variation in φ_0 among species. This result contrasts with the findings of (Björkman & Demmig, 1987), (Walker, 1992) and (Long *et al.*, 1993) who suggest an almost constant φ_0 among all species, regardless of their life-form. However, since our estimations were done at ecosystem scale, some of this difference could also reflect distinct canopy structures: a closed canopy would prevent leaves in the lower levels from being exposed to excessive light that could cause photodamage, thereby increasing the overall ecosystem-level φ_0 (Long *et al.*, 1994; Dashti *et al.*, 2025). Another source of variation could be attributed to different proportions of C3/C4 plants which have distinct φ_0 (Oberhuber *et al.*, 1993), with higher proportions of C4, eq. (5) might overestimate φ_0 in tropical grasslands and savannas due to C4 plants' low photorespiration.

Our findings of a universal peaked response to temperature are consistent with the predictions from the theory developed by (Johnson & Berry, 2021) (Fig 8c) – supporting the idea that the bell-shaped response of φ_0 to temperature is a general plant response which propagates to the ecosystem, thus creating a general ecosystem response to temperature.

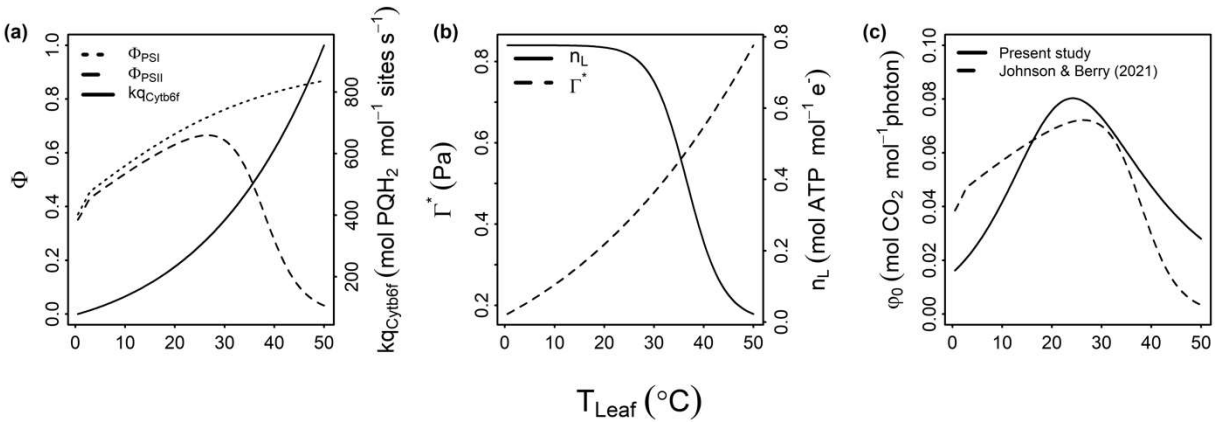

Fig. 8. Theoretical responses of selected electron-transport chain components to temperature, following Johnson & Berry (2021). Simulations were carried out under non-photorespiratory conditions: CO_2 = 700 μmol mol^{-1}, pO_2 = 2029 Pa, and low light (150 μmol m^{-2} s^{-1}). **(a)** Efficiencies of photosystems I and II and the catalytic constant for cytochrome b_6f. **(b)** The photorespiratory compensation point and the coupling efficiency of linear electron flow to the proton circuit (**η**L). **(c)** $\varphi_0(T)$ predictions from theory and from the present study.

In the Johnson-Berry theory, cytochrome b_6f (Cyt b_6f) modulates the transfer of electrons from plastoquinol (PQH2) to oxidized plastocyanin (PCox) at a rate *kq* (Fig. 8a), redistributing excitation energy between photosystems and diverting energy to thermal dissipation. Cyt b_6f also couples this electron transfer to the proton circuit from the stroma into the lumen, modulating the coupling between linear and cyclic electron flux (Johnson & Berry, 2021). When light is limiting, Cyt b_6f activity is at its maximum and so *kq* depends primarily on temperature, following a regular Arrhenius response. Most of the electron flow passing through Cyt b_6f, at limiting light, and connecting to the proton circuit, is thought to be linear; this efficiency decays exponentially at high temperatures (Fig. 8b) (Johnson & Berry, 2021).

Low φ_0 at low temperature could be explained by the accumulation of sustained non-photochemical quenching (NPQ) (Porcar-Castell, 2011) or by the rate of repair of photosystem II, which slows down at low temperature (Greer *et al.*, 1986; Mattila *et al.*, 2020). If this rate of repair becomes slower than the rate of PSII damage, it could lead to photoinhibition even under low light (Osmond, 1994; Tyystjärvi & Aro, 1996). This damage-repair imbalance is also documented when the rate of damage is enhanced by high temperature (Murata *et al.*, 2007; Sage & Kubien, 2007). It has been reported that PSI activity decreases at low temperatures only in

cold-sensitive plants (Sonoike, 1999), otherwise it is thermally stable. Its inactivation does not occur before the complete inactivation of PSII (Berry & Bjorkman, 1980; Oberhuber & Edwards, 1993).

Although we corrected for stomatal closure and photorespiration, implicitly accounting for Rubisco deactivation at high temperature, other factors could affect $\varphi_0(T)$ such as the solubility of CO_2 in water: this decreases as temperature increases, reducing the CO_2 concentration in C_3 plants and favouring oxygenation by Rubisco, as noted by (Ehleringer & Björkman, 1977). However, this effect is counterbalanced by the increase in CO_2 diffusivity and hence the increase of mesophyll conductance (von Caemmerer & Evans, 2015).

According to Eq. (6), respiration offsets the light response curve in each temperature bin without affecting the slope φ_0. Nonetheless, we double-checked our results by repeating the analysis using GPP from the FLUXNET dataset and setting respiration to zero, producing very similar results (Fig. S4).

Our results indicate that the maximum quantum efficiency $\hat{\varphi}_0$ at the ecosystem level decreases as climatological aridity increases, consistent with the observations of (Fu *et al.*, 2022) regarding the maximum evaporative fraction, and with (Mengoli *et al.*, 2023) regarding the maximum light-use efficiency of GPP. Several explanations are possible, including: (a) persistent effects of drought on the photosynthetic apparatus, such as damage to the light-harvesting complexes of PSII and reduction in the size of the PSI antenna (Hu *et al.*, 2023); (b) high leaf mass per area (LMA) (Wright *et al.*, 2004), typical in plants adapted to aridity, favouring photoprotective thermal dissipation over photochemistry (Adams *et al.*, 1987; Valladares *et al.*, 2000); (c) coordination of hydraulic and allocation traits (Flo *et al.*, 2021) such that plants of dry environments minimize hydraulic risk (Bassiouni *et al.*, 2023).

A few sites, however, showed relatively high $\hat{\varphi}_0$ at AI > 1. Although we cannot account for every case, there are many possible reasons why local conditions might differ from the bioclimate of the surrounding regions. For example, some sites such as AU-Lox (Stevens *et al.*, 2011) and US-KLS (Ji *et al.*, 2021) are irrigated; while others, such as SN-Dhr (Tagesson *et al.*, 2015) and US-Jo2 (Pérez-Ruiz *et al.*, 2022), experience a strong seasonal concentration of precipitation. Some sites have access to groundwater, like SD-Dem (Ardo *et al.*, 2008), or are man-made wetlands, like US-Myb (Eichelmann *et al.*, 2018). Other sites show a high PET/P ratio, but a significant portion of the energy is used for melting snow and thawing permafrost such as US-xHE (Osterkamp *et al.*, 2009) and US-Prr (Nakai *et al.*, 2013).

Activation energies for φ_0 showed little variation among sites; this is also the case for the activation energies of V_{cmax} and J_{max}, as reported by (Kattge & Knorr, 2007). ΔS decreases with increasing growth temperature, as also reported for V_{cmax} and J_{max} by (Kattge & Knorr, 2007) and (Kumarathunge *et al.*, 2019). Variation in ΔS shifts the optimum temperature by 0.35 ºC per degree of growth temperature and simultaneously reduces the sensitivity of φ_0 to T, as also noted by (Yin & Struik, 2009). This response is consistent with the observations of increased thermal stability of PSII at higher growth temperatures due to changes in thylakoid membrane lipids (Berry & Bjorkman, 1980). It is also consistent with the effect of higher growth temperatures on the accumulation of zeaxanthin, which enhances nonphotochemical quenching and thermal energy dissipation in PSII (Demmig-Adams *et al.*, 1989; Busch *et al.*, 2007). Overall, the variations of ΔS and $\widehat{\varphi_0}$ with $mGDD_0$ and aridity respectively support our general hypothesis that the temperature response of $\varphi_0(T)$ depends on adaptation to bioclimate.

We replicated our analysis on a year-by-year basis in sites with at least ten years of *in situ* fAPAR records (n = 3) (Fig. S1) and did not observe any signal of acclimation. While only three sites may not provide sufficient evidence, this observation is consistent with what was reported by (Bernacchi *et al.*, 2003). It would imply that the acclimation of V_{cmax} to temperature, which is a well-documented phenomenon (Medlyn *et al.*, 2002; Kattge & Knorr, 2007), does not apply to φ_0. However, some studies have reported acclimation to temperature of the initial slope of the light-response curve, such as (Dwyer *et al.*, 2007) and (Herrmann *et al.*, 2020). To our knowledge, only (Tenhunen *et al.*, 1976a) fitted the same equation as in this study and found variation of φ_0 with temperature – but the model presented there assumed constant φ_0 for simplicity.

Comparing our predictions with independent observations by (Rogers *et al.*, 2019) (Fig. 9) shows that considering the temperature dependency of φ_0 eliminates a general problem shared by TBMs, of overpredicting φ_0 at low temperatures. Our model also predicts a sharper decline in φ_0 at temperatures higher than T_{opt}. All else equal, this translates into a sharper decrease in assimilation at high temperatures.

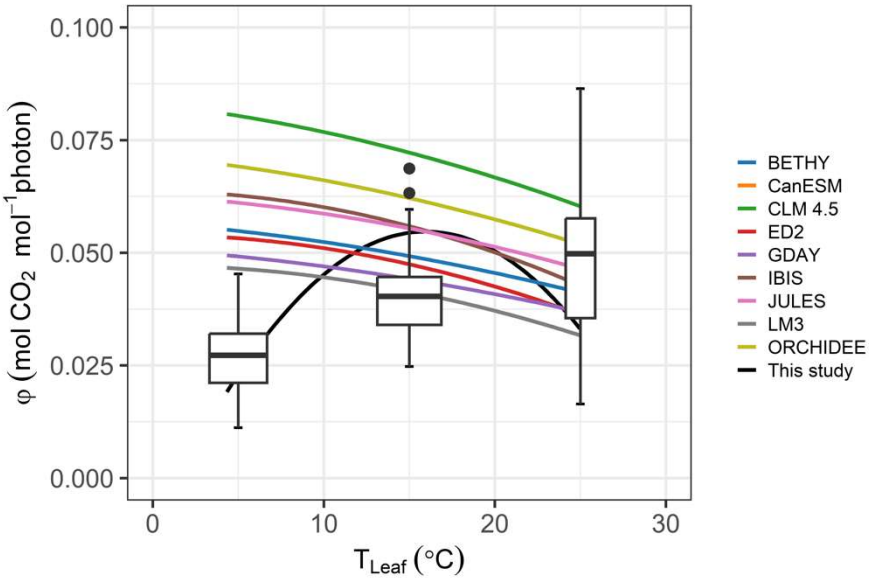

Fig. 9. Realized quantum efficiency of primary production as predicted by different models. The boxes and whiskers show measurements from (Rogers *et al.*, 2019) on Arctic plants; the black line shows results of our model. Results of other TBMs (coloured lines) are based on parameters and settings from (Rogers *et al.*, 2019).

When this new formulation, with global coefficients (Eqs. 6 to 9), was tested on the P-model without any soil moisture limitations, we simulated an increase in global total annual GPP from 114.3 ± 3.49 PgC yr^{-1} to 161.0 ± 4.38 PgC yr^{-1}, with respect to the original. The new value is closer to values inferred from ^{14}C (~160 PgC yr^{-1}), ^{18}O (150–175 PgC yr^{-1}) and carbonyl sulfide uptake, COS (157 ± 8.5 PgC yr^{-1}), but far from values derived from inverted soil respiration (149 ± 29 PgC yr^{-1}), and inferred from SIF (135.5 ± 8.8 PgC yr^{-1}) (Li & Xiao, 2019; Graven *et al.*, 2024; Lai *et al.*, 2024) (Fig. 10a). This change, however, was unevenly distributed; the increase was apparent in the tropical rainforests where the annual GPP increased by 1–3 kgC m^{-2} yr^{-1}, while in temperate and boreal forests the increment was moderated to ~0.5 kgC m^{-2} yr^{-1}. In arid regions, in contrast, there was a moderate decrease in modelled GPP (Fig 10b).

When we compared monthly LUE from the P-model with the original vs. the new φ_0 formulation, we saw an improvement in the R^2 from 0.16 to 0.21 (Fig 10d). However, the slope and the bias were degraded compared to the original. A possible reason is the fAPAR source. For example, (Stocker *et al.*, 2020) found a significant change in the magnitude of GPP when switching from MODIS fAPAR to fAPAR 3g. In our results, the underestimation occurs for high LUE values, which often represent tropical rainforests – where the error in remotely sensed fAPAR due to constant cloudiness is well documented (Zhang-Zheng *et al.*, 2024). It is worth noting that in (Stocker *et al.*, 2020) the same evaluation was done, but only roughly one-third of the data was available at that time; their R^2 was 0.31. In the same way, in our evaluation the original formulation was not able to surpass ~25 mmol mol^{-1} of monthly LUE (Fig 10c).

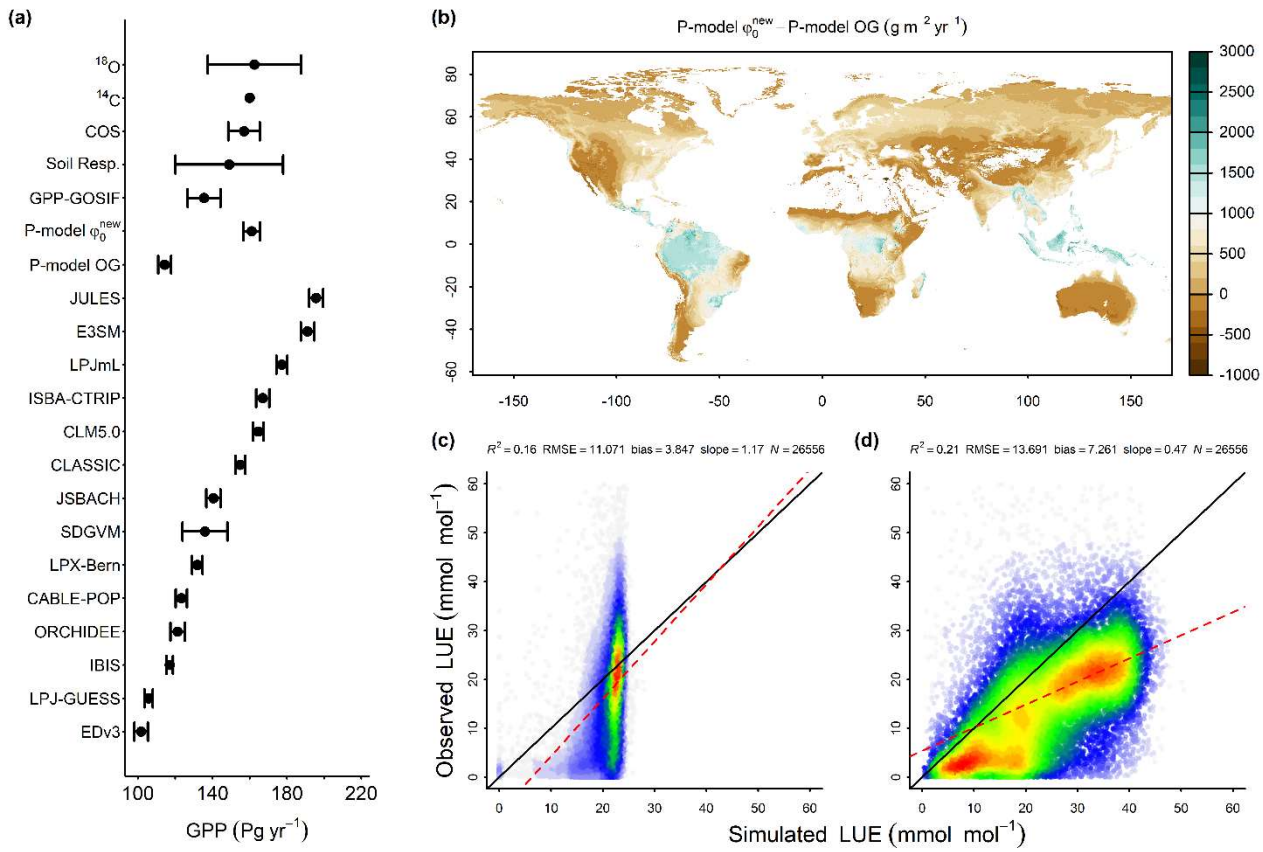

Fig. 10. φ_0 implementation in the P model. (a) Global mean annual GPP from different sources, including the TRENDY models (Sitch *et al.*, 2024) and this study. **(b)** Spatial distribution of the difference between global mean annual GPP, averaged over the years 2003 to 2020, from the new and the original P model ($\widehat{\varphi_0} = 0.087$ and f (T) from Bernacchi *et al.*, 2003). **(c)** Correlation of observed and simulated LUE monthly values using all the flux-tower data pooled, original P-model φ_0. **(d)** Correlation of observed and simulated LUE monthly values using all the flux tower data pooled and the new P model φ_0.

Overall, we have provided global evidence that φ_0 is not a fixed parameter (or fixed per plant functional type) as has been widely assumed in TBMs. Instead, it has a bell-shaped response to temperature, whose parameters are determined by bioclimatic adaptation. Incorporating these responses will be key to reliably assessing the response of the terrestrial biosphere to continuing climate change.

References

Adams WW, Smith SD, Osmond CB. **1987**. Photoinhibition of the CAM succulent Opuntia basilaris growing in Death Valley: evidence from 77K fluorescence and quantum yield. *Oecologia* **71**: 221–228.

Ardo J, Molder M, El-Tahir BA, Elkhidir HAM. **2008**. Seasonal variation of carbon fluxes in a sparse savanna in semi arid Sudan. *Carbon Balance and Management* **3**: 7.

Bao S, Wutzler T, Koirala S, Cuntz M, Ibrom A, Besnard S, Walther S, Šigut L, Moreno A, Weber U, *et al.* 2022. Environment-sensitivity functions for gross primary productivity in light use efficiency models. *Agricultural and Forest Meteorology* **312**.

Bassiouni M, Manzoni S, Vico G. **2023**. Optimal plant water use strategies explain soil moisture variability. *Advances in Water Resources* **173**.

Bernacchi CJ, Pimentel C, Long SP. **2003**. In vivo temperature response functions of parameters required to model RuBP-limited photosynthesis. *Plant, Cell and Environment* **26**: 1419–1430.

Berry JA, Bjorkman O. **1980**. Photosynthetic Response and Adaptation to Temperature in Higher Plants. *Annual Review of Plant Physiology* **31**: 491–543.

Bibi AC, Oosterhuis DM, Gonias ED. **2008**. Molecular biology amd physiology: Photosynthesis, quantum yield of photosystem II and membrane leakage as affected by high temperatures in cotton genotypes. *Journal of Cotton Science* **12**: 150–159.

Björkman O, Demmig B. **1987**. Photon yield of O_2 evolution and chlorophyll fluorescence characteristics at 77 K among vascular plants of diverse origins. *Planta* **170**: 489–504.

Bloomfield KJ, Stocker BD, Keenan TF, Prentice IC. **2023**. Environmental controls on the light use efficiency of terrestrial gross primary production. *Global Change Biology* **29**: 1037–1053.

Busch F, Hüner NPA, Ensminger I. **2007**. Increased air temperature during simulated autumn conditions does not increase photosynthetic carbon gain but affects the dissipation of excess energy in seedlings of the evergreen conifer jack pine. *Plant Physiology* **143**: 1242–1251.

von Caemmerer S. **2000**. *Biochemical models of leaf photosynthesis*. CSIRO.

von Caemmerer S, Evans JR. **2015**. Temperature responses of mesophyll conductance differ greatly between species. *Plant, Cell & Environment* **38**: 629–637.

Cao JJ, Chen J, Yang QP, Xiong YM, Ren WZ, Kong DL. **2022**. Leaf hydraulics coordinated with leaf economics and leaf size in mangrove species along a salinity gradient. *Plant Diversity*.

Carrara A, Kolari P, de Beeck MO, Arriga N, Berveiller D, Dengel S, Ibrom A, Merbold L, Rebmann C, Sabbatini S, *et al.* 2018. Radiation measurements at ICOS ecosystem stations.

International Agrophysics **32**: 589–605.

Dashti H, Chen M, Hao D, Yang X. **2025**. Canopy Structure Exhibits Linear and Nonlinear Links to Biome-Level Maximum Light Use Efficiency. *Ecology Letters* **28**.

Demmig-Adams B, Winter K, Krüger A, Czygan F-C. **1989**. Zeaxanthin and the Induction and Relaxation Kinetics of the Dissipation of Excess Excitation Energy in Leaves in 2% O 2 , 0% CO 2. *Plant Physiology* **90**: 887–893.

Dietze MC. **2014**. Gaps in knowledge and data driving uncertainty in models of photosynthesis. *Photosynthesis Research* **119**: 3–14.

Dwyer SA, Ghannoum O, Nicotra A, Von Caemmerer S. **2007**. High temperature acclimation of C 4 photosynthesis is linked to changes in photosynthetic biochemistry. *Plant, Cell and Environment* **30**: 53–66.

Ehleringer J, Björkman O. **1977**. Quantum Yields for CO2 Uptake in C3 and C4 Plants. *Plant Physiology* **59**: 86–90.

Ehleringer J, Pearcy RW. **1983**. Variation in Quantum Yield for CO2 Uptake among C3 and C4 Plants. *Plant Physiology* **73**: 555–559.

Eichelmann E, Hemes KS, Knox SH, Oikawa PY, Chamberlain SD, Sturtevant C, Verfaillie J, Baldocchi DD. **2018**. The effect of land cover type and structure on evapotranspiration from agricultural and wetland sites in the Sacramento–San Joaquin River Delta, California. *Agricultural and Forest Meteorology* **256–257**: 179–195.

Emerson R. **1958**. The Quantum Yield of Photosynthesis. *Annual Review of Plant Physiology* **9**: 1–24.

Evans J. **1987**. The Dependence of Quantum Yield on Wavelength and Growth Irradiance. *Australian Journal of Plant Physiology* **14**: 69–79.

Farquhar GD, Caemmerer S, Berry JA. **1980a**. A biochemical model of photosynthetic CO_2 assimilation in leaves of C_3 species. *Planta* **149**: 78-90–90.

Farquhar GD, von Caemmerer S, Berry JA. **1980b**. A biochemical model of photosynthetic CO2 assimilation in leaves of C3 species. *Planta* **149**: 78–90.

Feister U, Grewe R. **1995**. Spectral albedo measurements in the UV and visible region over different types of surfaces. *Photochemistry and Photobiology* **62**: 736–744.

Fisher JB, Huntzinger DN, Schwalm CR, Sitch S. **2014**. Modeling the Terrestrial Biosphere. *Annual Review of Environment and Resources* **39**: 91–123.

Flo V, Martínez-Vilalta J, Mencuccini M, Granda V, Anderegg WRL, Poyatos R. **2021**. Climate and functional traits jointly mediate tree water-use strategies. *New Phytologist* **231**: 617–630.

Fu Z, Ciais P, Feldman AF, Gentine P, Makowski D, Prentice IC, Stoy PC, Bastos A, Wigneron J-P. **2022**. Critical soil moisture thresholds of plant water stress in terrestrial ecosystems. *Science Advances* **8**: 1–13.

Genty B, Briantais JM, Baker NR. **1989**. The relationship between the quantum yield of photosynthetic electron transport and quenching of chlorophyll fluorescence. *Biochimica et Biophysica Acta - General Subjects* **990**: 87–92.

Graven HD, Warren H, Gibbs HK, Khatiwala S, Koven C, Lester J, Levin I, Spawn-Lee SA, Wieder W. **2024**. Bomb radiocarbon evidence for strong global carbon uptake and turnover in terrestrial vegetation. *Science (New York, N.Y.)* **384**: 1335–1339.

Greer DH, Berry JA, Björkman O. **1986**. Photoinhibition of photosynthesis in intact bean leaves: role of light and temperature, and requirement for chloroplast-protein synthesis during recovery. *Planta* **168**: 253–260.

Harrison SP, Cramer W, Franklin O, Prentice IC, Wang H, Brännström Å, de Boer H, Dieckmann U, Joshi J, Keenan TF, *et al.* 2021. Eco-evolutionary optimality as a means to improve vegetation and land-surface models. *New Phytologist* **231**: 2125–2141.

Herrmann HA, Schwartz JM, Johnson GN. **2020**. From empirical to theoretical models of light response curves - linking photosynthetic and metabolic acclimation. *Photosynthesis Research* **145**: 5–14.

Hill JF, Govindjee. **2014**. The controversy over the minimum quantum requirement for oxygen evolution. *Photosynthesis Research* **122**: 97–112.

Hu C, Elias E, Nawrocki WJ, Croce R. **2023**. Drought affects both photosystems in Arabidopsis thaliana. *New Phytologist* **240**: 663–675.

Hufkens K. **2022**. Flux data kit, a comprehensive data set of ecosystem fluxes for land surface modelling (v2.0) [Data set].

Ji L, Senay GB, Friedrichs M, Schauer M, Boiko O. **2021**. Characterization of water use and water balance for the croplands of Kansas using satellite, climate, and irrigation data. *Agricultural Water Management* **256**: 107106.

Johnson JE, Berry JA. **2021**. The role of Cytochrome b6f in the control of steady-state photosynthesis: a conceptual and quantitative model. *Photosynthesis Research* **148**: 101–136.

Johnson JE, Field CB, Berry JA. **2021**. The limiting factors and regulatory processes that control the environmental responses of C3, C3–C4 intermediate, and C4 photosynthesis. *Oecologia* **197**: 841–866.

Kattge J, Knorr W. **2007**. Temperature acclimation in a biochemical model of photosynthesis: a reanalysis of data from 36 species. *Plant, Cell & Environment* **30**: 1176–1190.

Kumarathunge DP, Medlyn BE, Drake JE, Tjoelker MG, Aspinwall MJ, Battaglia M, Cano FJ, Carter KR, Cavaleri MA, Cernusak LA, *et al.* 2019. Acclimation and adaptation components of the temperature dependence of plant photosynthesis at the global scale. *New Phytologist* **222**: 768–784.

Lai J, Kooijmans LMJ, Sun W, Lombardozzi D, Campbell JE, Gu L, Luo Y, Kuai L, Sun Y. **2024**. Terrestrial photosynthesis inferred from plant carbonyl sulfide uptake. *Nature* **634**.

Li X, Xiao J. **2019**. Mapping photosynthesis solely from solar-induced chlorophyll

fluorescence: A global, fine-resolution dataset of gross primary production derived from OCO-2. *Remote Sensing* **11**.

Long SP, Humphries S, Falkowski PG. **1994**. Photoinhibition of Photosynthesis in Nature. *Annual Review of Plant Physiology and Plant Molecular Biology* **45**: 633–662.

Long SP, Postl WF, Bolhár-Nordenkampf HR. **1993**. Quantum yields for uptake of carbon dioxide in C3 vascular plants of contrasting habitats and taxonomic groupings. *Planta* **189**: 226–234.

Mattila H, Mishra KB, Kuusisto I, Mishra A, Novotná K, Šebela D, Tyystjärvi E. **2020**. Effects of low temperature on photoinhibition and singlet oxygen production in four natural accessions of Arabidopsis. *Planta* **252**: 1–17.

McNeall D, Robertson E, Wiltshire A. **2024**. Constraining the carbon cycle in JULES-ES-1.0. *Geoscientific Model Development* **17**: 1059–1089.

Medlyn BE, Dreyer E, Ellsworth D, Forstreuter M, Harley PC, Kirschbaum MUF, Le Roux X, Montpied P, Strassemeyer J, Walcroft A, *et al.* 2002. Temperature response of parameters of a biochemically based model of photosynthesis. II. A review of experimental data. *Plant, Cell and Environment* **25**: 1167–1179.

Mengoli G, Harrison SP, Prentice IC. **2023**. A global function of climatic aridity accounts for soil moisture stress on carbon assimilation. *Preprint at https://doi.org/10.5194/egusphere-2023-1261*.

Muñoz-Sabater J. **2019**. ERA5-Land monthly averaged data from 1981 to present.

Murata N, Takahashi S, Nishiyama Y, Allakhverdiev SI. **2007**. Photoinhibition of photosystem II under environmental stress. *Biochimica et Biophysica Acta (BBA) - Bioenergetics* **1767**: 414–421.

Myneni RB, Knyazikhin Y, Park T. **2015**. MCD15A3H MODIS/Terra+Aqua Leaf Area Index/FPAR 4-day L4 Global 500m SIN Grid V006 [Data set].

Nakai T, Kim Y, Busey RC, Suzuki R, Nagai S, Kobayashi H, Park H, Sugiura K, Ito A. **2013**. Characteristics of evapotranspiration from a permafrost black spruce forest in interior Alaska. *Polar Science* **7**: 136–148.

Nash JE, Sutcliffe JV. **1970**. River flow forecasting through conceptual models part I — A discussion of principles. *Journal of Hydrology* **10**: 282–290.

Nelder JA, Mead R. **1965**. A Simplex Method for Function Minimization. *The Computer Journal* **7**: 308–313.

Neri P, Gu L, Song Y. **2024**. The effect of temperature on photosystem II efficiency across plant functional types and climate. *Biogeosciences* **21**: 2731–2758.

Novick KA, Biederman JA, Desai AR, Litvak ME, Moore DJP, Scott RL, Torn MS. **2018**. The AmeriFlux network: A coalition of the willing. *Agricultural and Forest Meteorology* **249**: 444–456.

Oberhuber W, Dai Z-Y, Edwards GE. **1993**. Light dependence of quantum yields of Photosystem II and CO2 fixation in C3 and C4 plants. *Photosynthesis Research* **35**: 265–274.

Oberhuber W, Edwards GE. **1993**. Temperature dependence of the linkage of quantum yield of photosystem II to CO2 fixation in C4 and C3 plants. *Plant Physiology* **101**: 507–512.

Osmond CB. **1994**. What is photoinhibition? Some insights from comparisons of shade and sun plants. In: Baker N, Bowyer J, eds. Photoinhibition: Molecular Mechanisms to the Field. Oxford, UK: Bios Scientific Publications, 1–24.

Osterkamp TE, Jorgenson MT, Schuur EAG, Shur YL, Kanevskiy MZ, Vogel JG, Tumskoy VE. **2009**. Physical and ecological changes associated with warming permafrost and thermokarst in Interior Alaska. *Permafrost and Periglacial Processes* **20**: 235–256.

Pastorello G, Trotta C, Canfora E, Chu H, Christianson D, Cheah Y-W, Poindexter C, Chen J, Elbashandy A, Humphrey M, *et al.* 2020. The FLUXNET2015 dataset and the ONEFlux processing pipeline for eddy covariance data. *Scientific Data* **7**: 225.

Pérez-Ruiz ER, Vivoni ER, Sala OE. **2022**. Seasonal carryover of water and effects on carbon dynamics in a dryland ecosystem. *Ecosphere* **13**: 1–14.

Porcar-Castell A. **2011**. A high-resolution portrait of the annual dynamics of photochemical and non-photochemical quenching in needles of Pinus sylvestris. *Physiologia Plantarum* **143**: 139–153.

Prentice IC, Liang X, Medlyn BE, Wang Y-P. **2015**. Reliable, robust and realistic: the three R's of next-generation land-surface modelling. *Atmospheric Chemistry and Physics* **15**: 5987–6005.

Rogers A, Medlyn BE, Dukes JS, Bonan G, von Caemmerer S, Dietze MC, Kattge J, Leakey ADB, Mercado LM, Niinemets Ü, *et al.* 2017. A roadmap for improving the representation of photosynthesis in Earth system models. *New Phytologist* **213**: 22–42.

Rogers A, Serbin SP, Ely KS, Wullschleger SD. **2019**. Terrestrial biosphere models may overestimate Arctic CO2 assimilation if they do not account for decreased quantum yield and convexity at low temperature. *New Phytologist* **223**: 167–179.

Sage RF, Kubien DS. **2007**. The temperature response of C 3 and C 4 photosynthesis. *Plant, Cell & Environment* **30**: 1086–1106.

Sandoval D, Prentice IC, Nóbrega RLB. **2024**. Simple process-led algorithms for simulating habitats (SPLASH v.2.0): robust calculations of water and energy fluxes. *Geoscientific Model Development* **17**: 4229–4309.

Singsaas EL, Ort DR, DeLucia EH. **2001**. Variation in measured values of photosynthetic quantum yield in ecophysiological studies. *Oecologia* **128**: 15–23.

Sitch S, O'Sullivan M, Robertson E, Friedlingstein P, Albergel C, Anthoni P, Arneth A, Arora VK, Bastos A, Bastrikov V, *et al.* 2024. Trends and Drivers of Terrestrial Sources and Sinks of Carbon Dioxide: An Overview of the TRENDY Project. *Global Biogeochemical Cycles* **38**: e2024GB008102.

Skillman JB. **2008**. Quantum yield variation across the three pathways of photosynthesis: Not yet out of the dark. *Journal of Experimental Botany* **59**: 1647–1661.

Smith EL. **1937**. The influence of light and carbon dioxide on photosynthesis. *Journal of General Physiology* **20**: 807–830.

Sonoike K. **1999**. The different roles of chilling temperatures in the photoinhibition of photosystem I and photosystem II. *Journal of Photochemistry and Photobiology B: Biology* **48**: 136–141.

Stevens RM, Ewenz CM, Grigson G, Conner SM. **2011**. Water use by an irrigated almond orchard. *Irrigation Science* **30**: 189–200.

Stocker BD, Wang H, Smith NG, Harrison SP, Keenan TF, Sandoval D, Davis T, Prentice IC. **2020**. P-model v1.0: an optimality-based light use efficiency model for simulating ecosystem gross primary production. *Geoscientific Model Development* **13**: 1545–1581.

Tagesson T, Fensholt R, Guiro I, Rasmussen MO, Huber S, Mbow C, Garcia M, Horion S, Sandholt I, Holm-Rasmussen B, *et al.* 2015. Ecosystem properties of semiarid savanna grassland in West Africa and its relationship with environmental variability. *Global Change Biology* **21**: 250–264.

Tenhunen JD, Weber JA, Yocum CS, Gates DM. **1976a**. Development of a photosynthesis model with an emphasis on ecological applications. II. Analysis of a data set describing the PM surface. *Oecologia* **26**: 101–119.

Tenhunen JD, Yocum CS, Gates DM. **1976b**. Development of a photosynthesis model with an emphasis on ecological applications - I. Theory. *Oecologia* **26**: 89–100.

Tyystjärvi E, Aro EM. **1996**. The rate constant of photoinhibition, measured in lincomycin-treated leaves, is directly proportional to light intensity. *PNAS* **93**: 2213–2218.

Ukkola AM, Abramowitz G, De Kauwe MG. **2022**. A flux tower dataset tailored for land model evaluation. *Earth System Science Data* **14**: 449–461.

Valladares F, Wright SJ, Lasso E, Kitajima K, Pearcy RW. **2000**. Plastic Phenotypic Response to Light of 16 Congeneric Shrubs from a Panamanian Rainforest. *Ecology* **81**: 1925.

Walker D. **1992**. Tansley Review No. 36 Excited leaves. *New Phytologist* **121**: 325–345.

Warburg O, Burk D, Schocken V, Hendricks SB. **1950**. The quantum efficiency of photosynthesis. *Biochimica et Biophysica Acta* **4**: 335–348.

Wright IJ, Reich PB, Westoby M, Ackerly DD, Baruch Z, Bongers F, Cavender-Bares J, Chapin T, Cornelissen JHC, Diemer M, *et al.* 2004. The worldwide leaf economics spectrum. *Nature* **428**: 821–827.

Yin X, Belay DW, Van Der Putten PEL, Struik PC. **2014**. Accounting for the decrease of photosystem photochemical efficiency with increasing irradiance to estimate quantum yield of leaf photosynthesis. *Photosynthesis Research* **122**: 323–335.

Yin X, Struik PC. **2009**. C3 and C4 photosynthesis models: An overview from the perspective

of crop modelling. *NJAS - Wageningen Journal of Life Sciences* **57**: 27–38.

Zhang Y, Kong D, Gan R, Chiew FHS, McVicar TR, Zhang Q, Yang Y. **2019**. Coupled estimation of 500 m and 8-day resolution global evapotranspiration and gross primary production in 2002–2017. *Remote Sensing of Environment* **222**: 165–182.

Zhang L-M, Yu G-R, Sun X-M, Wen X-F, Ren C-Y, Fu Y-L, Li Q-K, Li Z-Q, Liu Y-F, Guan D-X, *et al.* 2006. Seasonal variations of ecosystem apparent quantum yield (α) and maximum photosynthesis rate (Pmax) of different forest ecosystems in China. *Agricultural and Forest Meteorology* **137**: 176–187.

Zhang-Zheng H, Deng X, Aguirre-Gutiérrez J, Stocker BD, Thomson E, Ding R, Adu-Bredu S, Duah-Gyamfi A, Gvozdevaite A, Moore S, *et al.* 2024. Why models underestimate West African tropical forest primary productivity. *Nature Communications* **15**: 1–12.

Acknowledgments:

This work is a contribution to the LEMONTREE (Land Ecosystem Models based On New Theory, obseRvations and ExperimEnts) project. This research received support through Schmidt Sciences, LLC (Grant number G-21-61881: DSC, ICP, CM).

Author contributions:

Conceptualisation, coding and first draft writing: DS. All authors provided scientific input, reviewed and edited the final manuscript.

Competing interests:

Authors declare that they have no competing interests.

Data and materials availability:

All data, is freely available at

The code is available at

Supplementary Material